PAPER Special Section on Analog Circuit Techniques and Related Topics

Effects of Parasitic Elements on L-Type LC/CL Matching Circuits

Satoshi TANAKA[†a)], ***Fellow***, **Takeshi YOSHIDA**[†], ***Member***, ***and*** **Minoru FUJISHIMA**[†], ***Fellow***

SUMMARY L-type LC/CL matching circuits are well known for their simple analytical solutions and have been applied to many radio-frequency (RF) circuits. When actually constructing a circuit, parasitic elements are added to inductors and capacitors. Therefore, each L and C element has a self-resonant frequency, which affects the characteristics of the matching circuit. In this paper, the parallel parasitic capacitance to the inductor and the series parasitic inductor to the capacitance are taken up as parasitic elements, and the details of the effects of the self-resonant frequency of each element on the S_{11}, voltage standing wave ratio (VSWR) and S_{21} characteristics are reported. When a parasitic element is added, each characteristic basically tends to deteriorate as the self-resonant frequency decreases. However, as an interesting feature, we found that the combination of resonant frequencies determines the VSWR and passband characteristics, regardless of whether it is the inductor or the capacitor.

key words: *matching circuit, parasitic element, analytical solution, LC/CL, matching network*

1. Introduction

The L-type LC/CL matching circuit is well known for its simple analytical solution and has been applied to many radio frequency (RF) circuits [1]. A lot of research has been done on the design method when this is multi-staged [2]–[10]. In the actual circuit, parasitic elements are added to inductors and capacitors. When designing amplifiers, they are combined with transistors, and the input/output capacitor of the transistors can also be regarded as a kind of parasitic elements. However, the effect of adding a parasitic element to each element has not been studied much [11]. Of course, with today's advanced simulators, it is easy to design matching circuits that take into account the effects of parasitic elements. However, analytical understanding of the effects of parasitic elements is very effective in solving problems during design.

The design including parasitic elements is illustrated in Fig. 1. Figure 1(a) shows the interstage matching circuit of a typical integrated multistage complementary metal-oxide-semiconductor field effect transistor (CMOSFET) amplifier [12]. the CMOSFET has gate-to-source capacitance C_{GS}, gate-to-drain capacitance C_{GD}, and drain-to-source capacitance C_{DS}. The two FETs are connected by a π-type matching circuit consisting of LCL. Drain bias and gate bias are applied through the respective inductors L_1 and L_2; the drain

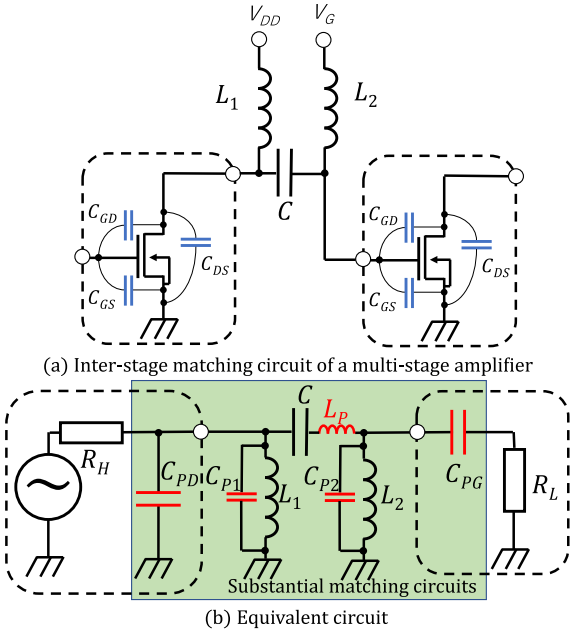

Fig. 1 Inter-stage matching circuit of a CMOS multi-stage amplifier and its equivalent circuit.

output impedance and gate input impedance of the CMOSFETs are both complex impedances. As shown in Fig. 1(b), the drain output impedance can be simply represented by the parallel connection of the output resistor R_H and the output capacitor C_{PD}. The gate input impedance can be represented by the series connection of the input resistor R_L and the input capacitor C_{PG}. When integrated capacitance is applied, a series parasitic inductor L_P is added due to the presence of series wiring. When integrated inductors are used, parallel parasitic capacitance is added due to the presence of capacitance between wires [13]. These parasitic effects must also be taken into account in the design. Although the interstage matching circuit exists between two CMOSFETs, it is appropriate to add C_{PD} and C_{PG} to the matching circuit components and terminate both ends with R_H and R_L as shown in Fig. 1(b) in order to study the bandwidth. Thus, a realistic matching circuit should include parasitic elements.

In our first study, the influence of parasitic elements added to the matching elements was confirmed, focusing on LC matching circuits among the L-type LC/CL matching circuits, which are the basis of matching circuits [14]. In this paper, we further studied the effect of parasitic elements in L-type CL matching circuits. At the same time, we

Manuscript received May 22, 2023.
Manuscript revised September 12, 2023.
Manuscript publicized November 7, 2023.
[†]The authors are with Hiroshima University, Higashi-Hiroshima-shi, 180-8585 Japan.
a) E-mail: tana@hiroshima-u.ac.jp
DOI: 10.1587/transfun.2023GCP0004

also discussed the details of the influence of parasitic elements in LC/CL matching circuits. Specifically, a parallel parasitic capacitance is added to the inductor element, and a series parasitic inductor is added to the capacitor. Furthermore, we obtained an analytical solution for the matching conditions in this case, and confirmed the effects of changes in the parasitic element values on the S_{11}, voltage standing wave ratio (VSWR), and S_{21} characteristics.

The element value was changed by changing the self-resonant frequency of each matching element when the parasitic element was included, rather than by directly changing the value of the parasitic element.

2. L-Type LC/CL Matching Circuits

Table 1 summarizes the circuit configuration of the LC/CL matching circuit and analytical matching conditions [9], [14], [15]. The LC matching circuit shown on the left in Table 1 is a matching circuit with low-pass characteristics, and is an L-type matching circuit consisting of a series inductor L and grounding capacitance C. The CL matching circuit shown on the right side of Table 1 is a matching circuit with high-pass characteristics, and is an L-type matching circuit consisting of a series capacitor C and a grounded inductor L. Input termination resistor R_L and output termination resistor R_H are connected to both matching circuits, and when $R_L < R_H$, matching can be achieved with appropriate L and C values.

In order to compare the characteristics of the LC/CL matching circuits, S_{11} on the input terminal side was calculated and shown in Fig. 2, assuming $R_L = 5\,\Omega$ and $R_H = 15\,\Omega$ under the conditions normalized to the matching frequency $f_0 = 1$ Hz. In the case of the LC matching circuit, the impedance of the series inductor is sufficiently small at low frequencies, and R_H can be seen directly. As the frequency increases, the reactance passes through the negative region and approaches R_L, and at 1 Hz, it can be matched to R_L. As the frequency rises further, the impedance of the inductor increases, and the reactance component passes through the positive region and becomes ∞.

In the case of the CL matching circuit, the impedance of the series capacitance is sufficiently large at low frequencies, and the impedance becomes ∞. As the frequency increases, the reactance passes through the negative region and approaches R_L, and at 1 Hz, it can be matched to R_L. As the frequency rises further, the impedance of the series capacitance becomes sufficiently small, and R_H can be seen directly through the region where the reactance component is positive.

Figure 3 shows the frequency dependence of the VSWR characteristics. Here we assume that the target specification is VSWR < 1.2. LC matching circuits that approach R_H at frequencies lower than 1 Hz satisfy the target specification over a wider bandwidth than CL matching circuits when compared below 1 Hz. Conversely, a CL matching circuit that approaches R_H at a frequency higher than 1 Hz satisfies the target specification over a wider bandwidth than an LC matching circuit when compared to a CL matching circuit at over 1 Hz.

Figure 4 shows the frequency dependence of S_{21}. Assume the target specification is $S_{21} > -0.3$ dB. As with the VSWR characteristics, the LC matching circuit, which approaches R_H at frequencies lower than 1 Hz, satisfies the target specification over a wider bandwidth than the CL matching circuit in the region below 1 Hz. Conversely, the CL matching circuit, which approaches R_H at frequencies higher than 1 Hz, satisfies the target specification over a

Table 1 The circuit configuration of the LC/CL matching circuit and analytical matching conditions Copyright © 2023, IEEE [14].

TYPE	LC matching circuits	CL matching circuits
Circuits	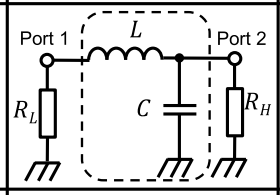	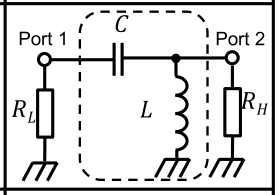
Matching condition	$L = \frac{1}{\omega_0}\sqrt{R_L(R_H - R_L)}$ $C = \frac{1}{\omega_0}\frac{1}{R_H}\sqrt{\frac{R_H - R_L}{R_L}}$	$C = \frac{1}{\omega_0}\frac{1}{\sqrt{R_L(R_H - R_L)}}$ $L = \frac{1}{\omega_0}R_H\sqrt{\frac{R_L}{R_H - R_L}}$

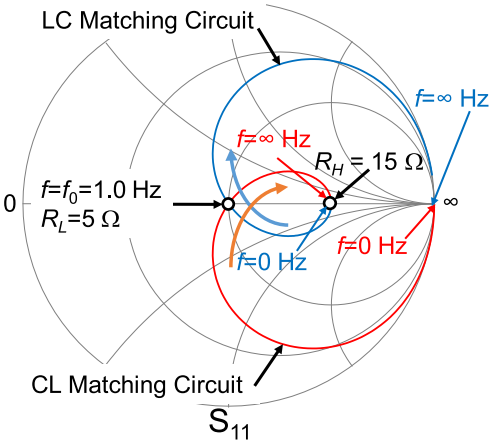

Fig. 2 Basic S_{11} characteristics of LC/CL matching circuits Copyright © 2023, IEEE [14].

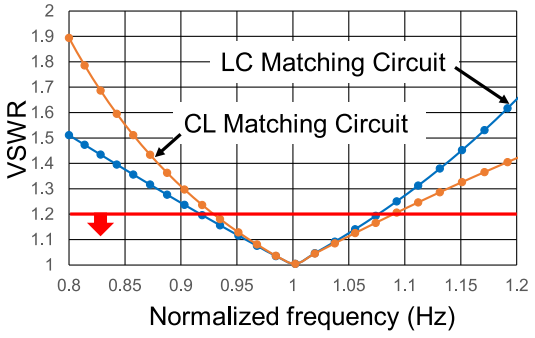

Fig. 3 VSWR characteristics of LC/CL matching circuits.

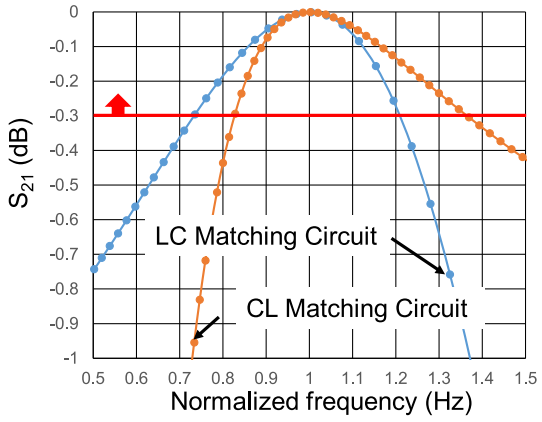

Fig. 4 S_{21} characteristics of LC/CL matching circuits.

Table 2 Parameter & performance comparison of LC/CL matching circuits.

Type	Items	L (H)	C (F)	$fmin$ (Hz)	$fmax$ (Hz)	fc (Hz)	FBW (%)	BW (Hz)
LC	VSWR<1.2	1.125	0.015	0.918	1.08	0.997	15.9	0.162
	S_{21}>-0.3 dB			0.73	1.21	0.971	49.5	0.48
CL	VSWR<1.2	1.688	0.023	0.931	1.084	1.007	15.2	0.153
	S_{21}>-0.3 dB			0.827	1.36	1.09	48.9	0.533

wider bandwidth than the LC matching circuit in the region above 1 Hz.

Table 2 summarizes the comparison of the characteristics of LC/CL matching circuits. The element value that realizes the matching condition at the same frequency is small for the element of the LC matching circuit. The fractional bandwidth (FBW) that satisfies VSWR $<$ 1.2 or $S_{21} > -0.3$ dB are almost the same for both. As for S_{21}, it can be seen that the CL matching circuit has a wider bandwidth (BW) defined by the difference between the maximum frequency f_{max} and the minimum frequency f_{min} that satisfy the conditions. However, since the center frequency fc of the band shifts to the region of $f_C < 1$ Hz in the LC matching circuit and shifts to the region of $f_C > 1$ Hz in the CL matching circuit, they are almost the same when compared in terms of FBW.

3. Analytical Solutions with Parasitic Elements

Table 3 summarizes the connection of parasitic elements. A parallel parasitic capacitance C_P is added to the inductor, and a series parasitic inductor L_P is added to the capacitor.

As shown in the third row of Table 3, the following two conditions must be satisfied at $f_0 = 1$ Hz in order to satisfy the matching condition even if the parasitic element is added. The first is that the impedance of the parallel connection of the capacitors C_P and L_a matches the original L. The second is that the impedance of the series connection of L_P and C_a matches the original C. The fourth row shows an analytical solution that is consistent with the case without parasitic elements. L_a and C_P, C_a and L_P are formulated using the original L and C value and the self-resonant frequencies ω_{RL} and ω_{RC}. Substituting the relationship described in the fourth row of Table 3 into the matching condition described

Table 3 Parasitic element of inductor and capacitor.

Element without parasitic	L	C
Element with parasitic	L_a, C_P	C_a, L_P
Conditions for the element values to be the same	$j\omega_0 L = \frac{1}{\frac{1}{j\omega_0 L_a} + j\omega_0 C_P}$ $\omega_{RL} = \frac{1}{\sqrt{L_a C_P}}$	$\frac{1}{j\omega_0 C} = \frac{1}{j\omega_0 C_a} + j\omega_0 L_P$ $\omega_{RC} = \frac{1}{\sqrt{L_P C_a}}$
Analytical solutions	$L_a = L\left(1 - \frac{\omega_0^2}{\omega_{RL}^2}\right)$ $C_P = \frac{1}{L(\omega_{RL}^2 - \omega_0^2)}$	$C_a = C\left(1 - \frac{\omega_0^2}{\omega_{RC}^2}\right)$ $L_P = \frac{1}{C(\omega_{RC}^2 - \omega_0^2)}$

Table 4 Analytical solution of the matching condition with parasitic elements Copyright © 2023, IEEE [14].

TYPE	LC matching circuits	CL matching circuits
Circuits	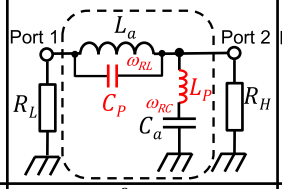	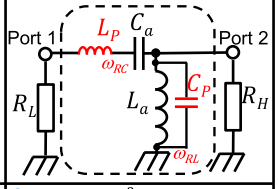
Matching condition	L $L_a = \frac{1-\frac{\omega_0^2}{\omega_{RL}^2}}{\omega_0}\sqrt{R_L(R_H - R_L)}$ $C_P = \frac{\omega_0}{\omega_{RL}^2 - \omega_0^2}\frac{1}{\sqrt{R_L(R_H - R_L)}}$ C $C_a = \frac{1-\frac{\omega_0^2}{\omega_{RC}^2}}{\omega_0}\frac{1}{R_H}\sqrt{\frac{R_H - R_L}{R_L}}$ $L_P = \frac{\omega_0}{\omega_{RC}^2 - \omega_0^2}R_H\sqrt{\frac{R_L}{R_H - R_L}}$	C $C_a = \frac{1-\frac{\omega_0^2}{\omega_{RC}^2}}{\omega_0}\frac{1}{\sqrt{R_L(R_H - R_L)}}$ $L_P = \frac{\omega_0}{\omega_{RC}^2 - \omega_0^2}\sqrt{R_L(R_H - R_L)}$ L $L_a = \frac{1-\frac{\omega_0^2}{\omega_{RL}^2}}{\omega_0}R_H\sqrt{\frac{R_L}{R_H - R_L}}$ $C_P = \frac{\omega_0}{\omega_{RL}^2 - \omega_0^2}\frac{1}{R_H}\sqrt{\frac{R_H - R_L}{R_L}}$

in Table 1, Table 4 summarizes the analytical solution of the matching condition when the parasitic element is included [14]. Each element is determined using this analytical solution, and the characteristics of the matching circuit at the self-resonant frequency are investigated. Filters that combine parallel and series resonators are well known [16], [17], but there is not much discussion about matching circuits.

4. Effects of Parasitic Elements on L-Type LC Matching Circuit Characteristics

Table 5 summarizes changes in the VSWR characteristics and passband characteristics (S_{21}) when the LC matching circuit has a self-resonant frequency due to the addition of parasitic elements. Four conditions are set for the self-resonant frequency f_{RL} of the inductor: 2 Hz, 3 Hz, 4 Hz, and ∞ (in the absence of parasitic elements).

Four conditions are set for the self-resonant frequency f_{RC} of the capacitor: 2 Hz, 3 Hz, 4 Hz, and ∞ (in the absence of parasitic elements). By combining these, the characteristics were confirmed under a total of 16 conditions.

Table 5 FBW of VSWR and S_{21} performances with parasitic elements on LC matching circuit.

f_{RL} \ f_{RC}		2				3				4				∞			
2		f_{rmin}	0.95	f_{pmin}	0.82	f_{rmin}	0.94	f_{pmin}	0.80	f_{rmin}	0.94	f_{pmin}	0.79	f_{rmin}	0.94	f_{pmin}	0.78
		f_{rmax}	1.04	f_{pmax}	1.11	f_{rmax}	1.05	f_{pmax}	1.13	f_{rmax}	1.05	f_{pmax}	1.14	f_{rmax}	1.05	f_{pmax}	1.14
		$f_{rcenter}$	1.00	$f_{pcenter}$	0.96	$f_{rcenter}$	1.00	$f_{pcenter}$	0.96	$f_{rcenter}$	1.00	$f_{pcenter}$	0.96	$f_{rcenter}$	1.00	$f_{pcenter}$	0.96
		FBW (%)	9.49	FBW (%)	30.8	FBW (%)	10.9	FBW (%)	34.7	FBW (%)	11.3	FBW (%)	35.9	FBW (%)	11.8	FBW (%)	37.4
3		f_{rmin}	0.94	f_{pmin}	0.80	f_{rmin}	0.93	f_{pmin}	0.77	f_{rmin}	0.93	f_{pmin}	0.76	f_{rmin}	0.93	f_{pmin}	0.75
		f_{rmax}	1.05	f_{pmax}	1.13	f_{rmax}	1.06	f_{pmax}	1.16	f_{rmax}	1.06	f_{pmax}	1.17	f_{rmax}	1.07	f_{pmax}	1.18
		$f_{rcenter}$	1.00	$f_{pcenter}$	0.96	$f_{rcenter}$	1.00	$f_{pcenter}$	0.96	$f_{rcenter}$	1.00	$f_{pcenter}$	0.96	$f_{rcenter}$	1.00	$f_{pcenter}$	0.97
		FBW (%)	10.9	FBW (%)	34.8	FBW (%)	12.8	FBW (%)	40.1	FBW (%)	13.4	FBW (%)	41.9	FBW (%)	14.1	FBW (%)	44.0
4		f_{rmin}	0.94	f_{pmin}	0.79	f_{rmin}	0.93	f_{pmin}	0.76	f_{rmin}	0.93	f_{pmin}	0.75	f_{rmin}	0.92	f_{pmin}	0.74
		f_{rmax}	1.05	f_{pmax}	1.14	f_{rmax}	1.06	f_{pmax}	1.17	f_{rmax}	1.07	f_{pmax}	1.18	f_{rmax}	1.07	f_{pmax}	1.19
		$f_{rcenter}$	1.00	$f_{pcenter}$	0.96	$f_{rcenter}$	1.00	$f_{pcenter}$	0.96	$f_{rcenter}$	1.00	$f_{pcenter}$	0.97	$f_{rcenter}$	1.00	$f_{pcenter}$	0.97
		FBW (%)	11.3	FBW (%)	36.0	FBW (%)	13.4	FBW (%)	41.9	FBW (%)	14.1	FBW (%)	43.8	FBW (%)	14.9	FBW (%)	46.2
∞		f_{rmin}	0.94	f_{pmin}	0.78	f_{rmin}	0.93	f_{pmin}	0.75	f_{rmin}	0.92	f_{pmin}	0.74	f_{rmin}	0.92	f_{pmin}	0.73
		f_{rmax}	1.05	f_{pmax}	1.14	f_{rmax}	1.07	f_{pmax}	1.18	f_{rmax}	1.07	f_{pmax}	1.19	f_{rmax}	1.08	f_{pmax}	1.21
		$f_{rcenter}$	1.00	$f_{pcenter}$	0.96	$f_{rcenter}$	1.00	$f_{pcenter}$	0.97	$f_{rcenter}$	1.00	$f_{pcenter}$	0.97	$f_{rcenter}$	1.00	$f_{pcenter}$	0.97
		FBW (%)	11.8	FBW (%)	37.4	FBW (%)	14.2	FBW (%)	44.0	FBW (%)	14.9	FBW (%)	46.2	FBW (%)	15.9	FBW (%)	49.0

The frequency response was calculated with 50 points per octave, and the frequencies that satisfy the specifications of VSWR ≤ 1.2 and $S_{21} \geq -0.3$ were obtained by linear completion.

The band that satisfies VSWR ≤ 1.2 (minimum frequency f_{rmin} and maximum frequency f_{rmax}), its center frequency $f_{rcenter}$ and FBR (fractional bandwidth), and the band that satisfies $S_{21} \geq -0.3$ dB (minimum frequency f_{pmin} and maximum frequency f_{pmax}) and its center frequency $f_{pcenter}$ and FBW were confirmed.

It can be seen that both bands widen as the self-resonant frequency increases. It was also found that when the self-resonant frequency is four times or less than the design frequency, band deterioration due to parasitic elements becomes apparent. An interesting characteristic is that even if the combination of $f_{RL} = 2$ Hz, $f_{RC} = 3$ Hz and the combination of $f_{RL} = 3$ Hz, $f_{RC} = 2$ Hz are different, if the combination of self-resonant frequencies is the same, the characteristics will be the same (although there are small calculation errors in the results in Table 5).

The details of the characteristics are explained using Figs. 5–8 [14]. Figure 5 shows the S_{11} characteristics on the input side. The frequency was varied in the range of 0.01–10.0 (Hz). In the absence of parasitic elements, as shown in Fig. 2, the input resistance is 15 Ω when the frequency is 0, 5 Ω when the frequency is 1 Hz, and converges to ∞ when the frequency increases.

As shown by the purple curve, when $f_{RL} = 2$ Hz and $f_{RC} = 3$ Hz, it shifts outward at frequencies below 1 Hz and shifts inward at frequencies above 1 Hz compared to the case without parasitic elements. It becomes ∞ at $f = f_{RL} = 2$ Hz. At $f = f_{RC} = 3$ Hz, the output resistor R_H is terminated to GND (See also Table 3), and the input impedance becomes the capacitive impedance of the parallel resonant circuit of L_a and C_P. As shown by the green curve, when $f_{RL} = 3$ Hz and $f_{RC} = 2$ Hz, it shifts inward at frequencies below 1 Hz and shifts outward at frequencies above 1 Hz compared to the case without parasitic elements. At $f = f_{RC} = 2$ Hz, the output resistor R_H is terminated to the GND and the input impedance becomes the inductive impedance of the parallel-resonant circuit of L_a and C_P. The input impedance becomes ∞ at $f = f_{RL} = 3$ Hz.

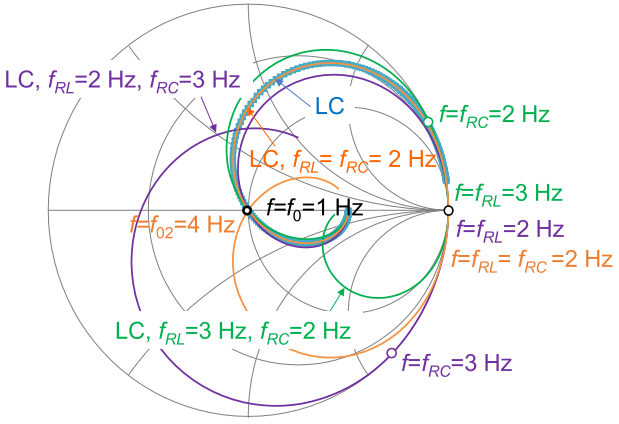

Fig. 5 S_{11} characteristics on the input side of L-type LC matching circuit with parasitic elements Copyright © 2023, IEEE [14].

As shown by the orange curve, when $f_{RL} = f_{RC} = 2$ Hz, it follows the locus without parasitic elements as the frequency changes. However, the input impedance becomes ∞ at $f = 2$ Hz. As the frequency is further increased, it gradually approaches the origin, matching 5 Ω at $f = f_{02} = 4$ Hz, and as the frequency is further increased, it approaches 15 Ω.

Next, focus on the VSWR frequency characteristics shown in Fig. 6 and the S_{21} frequency characteristics shown in Fig. 7. With parasitic elements, the band that satisfies VSWR ≦ 1.2 and $S_{21} \geqq -0.3$ dB becomes narrower than without parasitic elements.

The VSWR and S_{21} characteristics are the same for $f_{RL} = 2$ Hz, $f_{RC} = 3$ Hz and $f_{RL} = 3$ Hz, $f_{RC} = 2$ Hz, where the trajectories on S_{11} are different. The narrowest band is obtained under the condition of $f_{RL} = f_{RC} = 2$ Hz where the locus on S_{11} overlaps with the case without parasitic elements.

Figure 8 shows the expanded frequency range of the frequency characteristics of S_{21}. Under the conditions of $f_{RL} = 2$ Hz, $f_{RC} = 3$ Hz and $f_{RL} = 3$ Hz, $f_{RC} = 2$ Hz, Under the condition of $f = 2, 3$ Hz, S_{21} is 0 in true value and theoretically $-\infty$ dB in dB expression. This is due to the parallel and series resonance of the elements including their

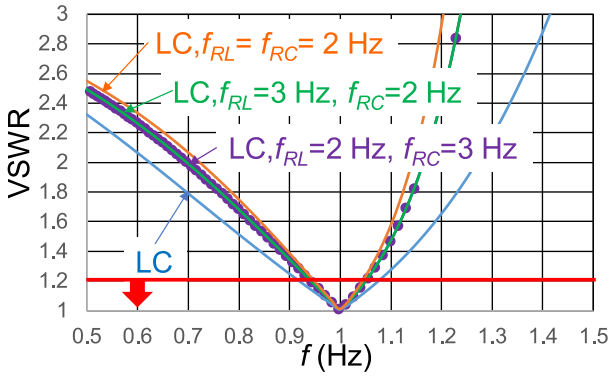

Fig. 6 VSWR characteristics on the input side of L-type LC matching circuit with parasitic elements Copyright © 2023, IEEE [14].

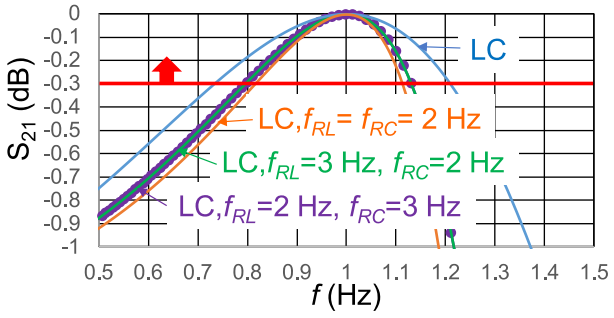

Fig. 7 S_{21} characteristics of L-type LC matching circuit with parasitic elements Copyright © 2023, IEEE [14].

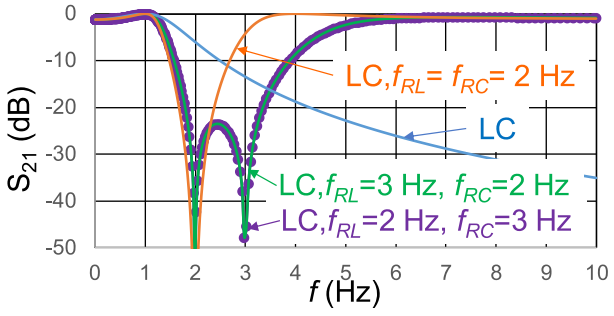

Fig. 8 S_{21} characteristics L-type LC matching circuit with parasitic elements on wider frequency range Copyright © 2023, IEEE [14].

respective parasitic elements. It also has a large attenuation between 2 Hz and 3 Hz.

It should be noted that the combination of matching characteristics differs depending on the items to be evaluated.

5. Effects of Parasitic Elements on L-Type CL Matching Circuit Characteristics

Table 6 summarizes changes in the VSWR characteristics and passband characteristics (S_{21}) when the CL matching circuit has a self-resonant frequency due to the addition of parasitic elements. Four conditions are set for the self-resonant frequency f_{RL} of the inductor: 2 Hz, 3 Hz, 4 Hz,

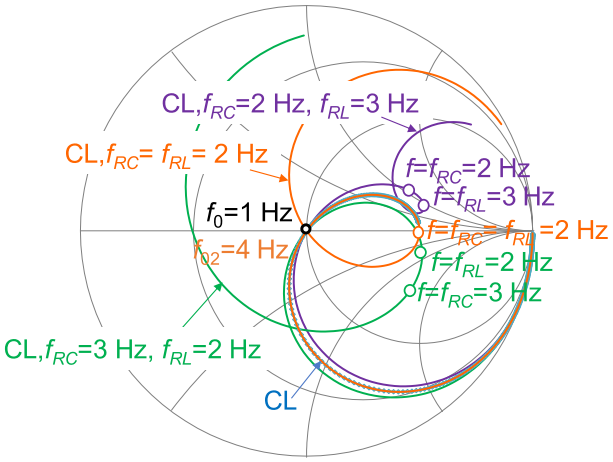

Fig. 9 S_{11} characteristics on the input side of L-type CL matching circuit with parasitic elements.

and ∞ (in the absence of parasitic elements). Four conditions are set for the self-resonant frequency f_{RC} of the capacitor: 2 Hz, 3 Hz, 4 Hz, and ∞ (in the absence of parasitic elements).

Using the same notation as in Table 4, by combining these, the characteristics were confirmed under a total of 16 conditions. It can be seen that both bands widen as the self-resonant frequency increases. It was also found that when the self-resonant frequency is four times or less than the design frequency, band deterioration due to parasitic elements becomes apparent. An interesting characteristic is that even if the combination of f_{RC} = 2 Hz, f_{RL} = 3 Hz and the combination of f_{RC} = 3 Hz, f_{RL} = 2 Hz are different, if the combination of self-resonant frequencies is the same, the characteristics will be the same.

The details of the characteristics are explained using Figs. 9–12. Figure 9 shows the S_{11} characteristics on the input side. The frequency was varied in the range of 0.01–10.0. In the absence of parasitic elements, as shown in Fig. 2, the input resistance is ∞ when the frequency is 0, 5 Ω when the frequency is 1 Hz, and as the frequency is further increased, the impedance converges to 15 Ω.

As shown by the purple curve, when f_{RC} = 2 Hz and f_{RL} = 3 Hz, it shifts inward at frequencies below 1 Hz and shifts outward at frequencies above 1 Hz compared to the case without parasitic elements. Further increasing the frequency, the impedance increases after one rotation within a region where reactance is positive, eventually approaching ∞.

As shown by the green curve, when f_{RC} = 3 Hz and f_{RL} = 2 Hz, it shifts outward at frequencies below 1 Hz and shifts inward at frequencies above 1 Hz compared to the case without parasitic elements. As the frequency is further increased, the impedance moves from the area where reactance is positive to the negative, makes one rotation, and then returns to the area where reactance is positive again.

As shown by the orange curve, when f_{RC} = f_{RL} = 2 Hz, it follows the locus without parasitic elements as the fre-

Table 6 FBW of VSWR and S_{21} performances with parasitic elements on CL matching circuit.

f_{RC} \ f_{RL}		2				3				4				∞			
2		f_{rmin}	0.96	f_{pmin}	0.89	f_{rmin}	0.95	f_{pmin}	0.87	f_{rmin}	0.95	f_{pmin}	0.87	f_{rmin}	0.95	f_{pmin}	0.86
		f_{rmax}	1.05	f_{pmax}	1.18	f_{rmax}	1.06	f_{pmax}	1.21	f_{rmax}	1.06	f_{pmax}	1.22	f_{rmax}	1.06	f_{pmax}	1.23
		$f_{rcenter}$	1.00	$f_{pcenter}$	1.03	$f_{rcenter}$	1.00	$f_{pcenter}$	1.04	$f_{rcenter}$	1.00	$f_{pcenter}$	1.04	$f_{rcenter}$	1.01	$f_{pcenter}$	1.05
		FBW (%)	9.52	FBW (%)	28.6	FBW (%)	10.8	FBW (%)	32.5	FBW (%)	11.2	FBW (%)	33.7	FBW (%)	11.7	FBW (%)	35.0
3		f_{rmin}	0.95	f_{pmin}	0.87	f_{rmin}	0.94	f_{pmin}	0.86	f_{rmin}	0.94	f_{pmin}	0.85	f_{rmin}	0.94	f_{pmin}	0.84
		f_{rmax}	1.06	f_{pmax}	1.21	f_{rmax}	1.07	f_{pmax}	1.26	f_{rmax}	1.07	f_{pmax}	1.28	f_{rmax}	1.08	f_{pmax}	1.30
		$f_{rcenter}$	1.00	$f_{pcenter}$	1.04	$f_{rcenter}$	1.01	$f_{pcenter}$	1.06	$f_{rcenter}$	1.01	$f_{pcenter}$	1.06	$f_{rcenter}$	1.01	$f_{pcenter}$	1.07
		FBW (%)	10.8	FBW (%)	32.5	FBW (%)	12.7	FBW (%)	38.5	FBW (%)	13.3	FBW (%)	40.4	FBW (%)	14.1	FBW (%)	42.8
4		f_{rmin}	0.95	f_{pmin}	0.87	f_{rmin}	0.94	f_{pmin}	0.85	f_{rmin}	0.94	f_{pmin}	0.84	f_{rmin}	0.93	f_{pmin}	0.84
		f_{rmax}	1.06	f_{pmax}	1.22	f_{rmax}	1.07	f_{pmax}	1.28	f_{rmax}	1.08	f_{pmax}	1.30	f_{rmax}	1.08	f_{pmax}	1.33
		$f_{rcenter}$	1.00	$f_{pcenter}$	1.04	$f_{rcenter}$	1.01	$f_{pcenter}$	1.06	$f_{rcenter}$	1.01	$f_{pcenter}$	1.07	$f_{rcenter}$	1.01	$f_{pcenter}$	1.08
		FBW (%)	11.2	FBW (%)	33.7	FBW (%)	13.3	FBW (%)	40.4	FBW (%)	14.0	FBW (%)	42.7	FBW (%)	14.9	FBW (%)	45.5
∞		f_{rmin}	0.95	f_{pmin}	0.86	f_{rmin}	0.94	f_{pmin}	0.84	f_{rmin}	0.93	f_{pmin}	0.84	f_{rmin}	0.93	f_{pmin}	0.83
		f_{rmax}	1.06	f_{pmax}	1.23	f_{rmax}	1.08	f_{pmax}	1.30	f_{rmax}	1.08	f_{pmax}	1.33	f_{rmax}	1.09	f_{pmax}	1.36
		$f_{rcenter}$	1.01	$f_{pcenter}$	1.05	$f_{rcenter}$	1.01	$f_{pcenter}$	1.07	$f_{rcenter}$	1.01	$f_{pcenter}$	1.08	$f_{rcenter}$	1.01	$f_{pcenter}$	1.10
		FBW (%)	11.7	FBW (%)	35.0	FBW (%)	14.1	FBW (%)	42.8	FBW (%)	14.9	FBW (%)	45.5	FBW (%)	15.9	FBW (%)	49.0

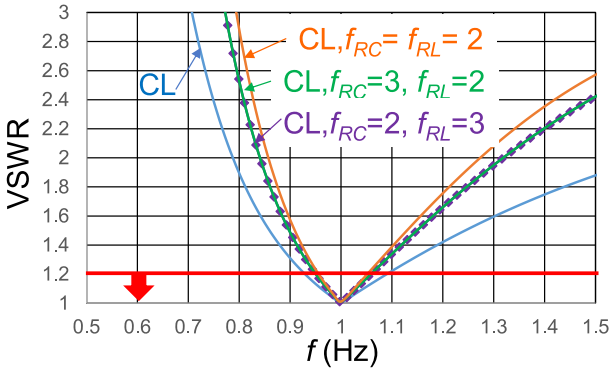

Fig. 10 VSWR characteristics on the input side of L-type CL matching circuit with parasitic elements.

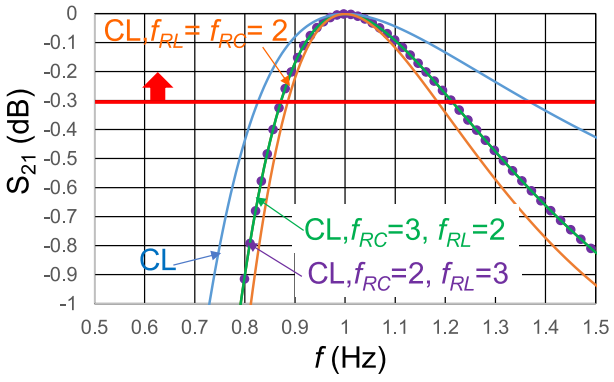

Fig. 11 S_{21} characteristics of L-type CL matching circuit with parasitic elements.

quency changes. However, the input impedance becomes 15 Ω at f = 2 Hz. As the frequency is further increased, the impedance moves into the negative reactance region and is again matched to 5 Ω at $f = f_{02}$ = 4 Hz. With further increase in frequency, reactance returns to the positive region again.

Next, focus on the VSWR frequency characteristics shown in Fig. 10 and the S_{21} frequency characteristics shown in Fig. 11. With parasitic elements, the band that satisfies.

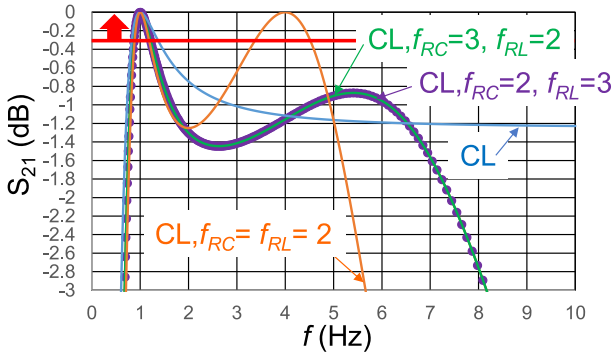

Fig. 12 S_{21} characteristics L-type CL matching circuit with parasitic elements on wider frequency range.

With parasitic elements, the band that satisfies VSWR ≦ 1.2 and S_{21} ≧ −0.3 dB becomes narrower than without parasitic elements.

The VSWR and S_{21} characteristics are the same for f_{RC} = 2 Hz, f_{RL} = 3 Hz and f_{RC} = 3 Hz, f_{RL} = 2 Hz, where the trajectories on S_{11} are different. The narrowest band is obtained under the condition of f_{RC} = f_{RL} = 2 Hz where the locus on S_{11} overlaps with the case without parasitic elements.

Figure 12 shows the expanded frequency range of the frequency characteristics of S_{21}. Under the conditions of f_{RL} = 2 Hz, f_{RC} = 3 Hz and f_{RL} = 3 Hz, f_{RC} = 2 Hz, After S_{21} = 0 dB at 1 Hz, S_{21} decreases as frequency is increased, then increases again, and finally decreases. Under the conditions of f_{RC} = f_{RL} = 2 Hz, S_{21} becomes 0 dB at f = 1, 4 Hz. After S_{21} = 0 dB at 1 Hz, S_{21} decreases as the frequency is increased, then increases again, and then S_{21} = 0 dB again at 4 Hz. Further increasing the frequency causes S_{21} to finally decrease.

6. Conclusion

We have confirmed the change in characteristics when a parasitic element is added to the L-type LC/CL matching circuit. A self-resonant frequency is generated in the inductor and the capacitor by adding the parasitic capacitance and the

parasitic inductor, respectively. As a common feature, when checking the bands of VSWR and S_{21}, it can be seen that both bands become narrower as the self-resonant frequency of the constituent elements is lowered. In addition, when the self-resonant frequency is changed from 2 to 4 times and confirmed, it was found that the frequency band of VSWR and S_{21} is the same with the same frequency combination regardless of whether the element is L or C.

In this first study, we analytically confirmed the details of the effect of parasitic elements added to the matching elements in the L-type LC/CL matching circuit, which is the basis of the matching circuit, and as a future issue, we will extend this study to a multistage LC/CL matching circuit as shown in Fig. 1. Note that the newly added L and C are treated here as parasitic elements. However, in harmonic control of power amplifiers, these elements may be intentionally added to the LC/CL matching circuit in order to short-circuit or open-circuit second-order or higher-order harmonics [18]–[22]. We believe this study is applicable to this case as well.

Acknowledgments

This research work was financially supported by the Ministry of Internal Affairs and Communications of Japan with a scheme of "Research and Development for Expansion of Radio Wave Resources" (JPJ000254).

References

[1] D.M. Pozar, Microwave Engineering, 4th ed, John Wiley & Sons, 2012.
[2] D. Fielder, "Broad-band matching between load and source systems," IRE Trans. on Circuit Theory, vol.8, no.2, pp.138–153, June 1961.
[3] G.L. Matthaei, "Tables of Chebyshev impedance-transforming networks of low-pass filter form," Proc. IEEE, vol.52, no.8, pp.939–963, Aug. 1964.
[4] E.G. Cristal, "Tables of maximally flat impedance-transforming networks of low-pass filter form (Correspondence)," IEEE Trans. Microw. Theory Techn., vol.13, no.5, pp.693–695, Sept. 1965.
[5] H. Dedieu, C. Dehollain, J. Neirynck, and G. Rhodes, "A new method for solving broadband matching problems," IEEE Trans. Circuit Syst. I, Fundam. Theory Appl., vol.41, no.9, pp.561–571, Sept. 1994.
[6] A. Kilinc and B.S. Yarman, "High precision LC ladder synthesis part I: Lowpass ladder synthesis via parametric approach," IEEE Trans. Circuit Syst. I, Reg. Papers, vol.60, no.8, pp.2074–2083, Aug. 2013.
[7] B.S. Yarman and A. Kilinc, "High precision LC ladder synthesis part II: Immittance synthesis with transmission zeros at DC and infinity," IEEE Trans. Circuit Syst. I, Reg. Papers, vol.60, no.10, pp.2719–2729, Oct. 2013.
[8] A. Ismail and A. Abidi, "A 3–10-GHz low-noise amplifier with wideband LC-ladder matching network," IEEE J. Solid-State Circuits, vol.39, no.12, pp.2269–2277, Dec. 2004
[9] S. Tanaka, "A new decomposition method of LC-ladder matching circuits with negative components," IEICE Trans. Fundamentals, vol.E103-A, no.9, pp.1011–1071, Sept. 2020.
[10] S. Tanaka, "Analysis on multi-stage LC ladder matching circuits with complex terminated LC and CL circuits," IEICE Trans. Fundamentals, vol.E104-A, no.11, pp.1451–1461, Nov. 2021.
[11] B. Gowrish, K. Rawat, A. Basu, and S.K. Koul, "Broad-band matching network using band-pass filter with device parasitic absorption," IEEE 82nd ARFTG Microwave Measurement Conference, pp.1–4, Nov. 2013.
[12] S. Yabuki, S. Fujimoto, S. Amakawa, T. Yoshida, and M. Fujishima, "29-to-65-GHz CMOS amplifier with tunable frequency response," IEEE RFIT2022 T4F.9, pp.63–65, Aug. 2022.
[13] B. Razavi, RF Microelectronics 2nd ed., Person Education, 2012.
[14] S. Tanaka, T. Yoshida, and M. Fujishima, "Effects of parasitic elements on LC/CL matching circuits," ITC-CSCC 2023, pp.1–4, June 2023.
[15] Y. Konishi, Introduction to Wireless Communication Circuits, Sogo-Shuppan-Sha, 1995.
[16] L. Besser and R. Gilmore, Practical RF Circuit Design for Modern Wireless Systems, Vol.1: Passive Circuits and Systems, Artech House, 2003.
[17] L.K. Yeung, K. Wu, and Y.E. Wang, "Low-temperature cofired ceramic LC filters for RF applications," IEEE Microw. Mag., vol.9, no.5, pp.118–128, Oct. 2008.
[18] A. Inoue, T. Heima, A. Ohta, R. Hattori, and Y. Mitsui, "Analysis of class-F and inverse class-F amplifiers," 2000 IEEE MTT-S Int. Microwave Symp. Dig., pp.775–778, June 2000.
[19] A. Ohta, A. Inoue, S. Goto, K. Ueda, T. Ishikawa, and Y. Masuda, "Intermodulation distortion analysis of class-F and inverse class-F HBT amplifiers," IEEE Trans. Microw. Theory Techn., vol.53, no.6, pp.2121–2128, June 2005.
[20] Y.Y. Woo, Y. Yang, and B. Kim, "Analysis and experiments for high-efficiency class-F and inverse class-F power amplifier," IEEE Trans. Microw. Theory Techn., vol.54, no.5, pp.1969–1974, May 2006.
[21] S. Tanaka, "Progress of the linear RF power amplifier for mobile phones," IEICE Trans. Fundamentals, vol.E101-A, no.2, pp.385–395, Feb. 2018.
[22] S.C. Cripps, RF Power Amplifier for Wireless Communications, 2nd ed., Artech House microwave library, 2006.

Satoshi Tanaka received the B.S. and M.S. degrees in electrical engineering from Waseda University, Tokyo, Japan, in 1983 and 1985, respectively, and the Ph.D. degree in communication engineering from Tohoku University, Miyagi, Japan, in 2019. In 1985, he joined the Central Research Laboratory, Hitachi, Ltd., Tokyo, Japan, where he was engaged in the research and development of mixed RF analog and digital bipolar CMOS, GaAs and Bi-CMOS RFICs for pager, PHS, RFID Tag, GSM and W-CDMA applications. From 1995 to 1996, he joined Integrated Circuits and Systems Lab., University of California, Los Angeles, US, as a visiting scholar where he worked for research on RF CMOS circuit for WLAN applications. In 2006, he moved to Renesas Technology Co., Tokyo, Japan, and developed a power amplifier for mobile phones using LDMOS and HBT. In 2012, he joined Murata Manufacturing Co., Ltd., Kyoto, Japan. He developed RF front-end modules, especially multiband multimode PA modules for GSM/W-CDMA/LTE/5G. In 2022, he joined Hiroshima University, Higashi-Hiroshima, Japan as a Special Appointed Professor. His current research interests include Sub-THz RF circuits and its applications. Dr. Tanaka was a Technical Committee Member of the IEEE International Conference on Solid-State Circuits (ISSCC) from 2005 to 2009. From 2009 to 2018, he was an RF program committee chair of the IEEE Asian Conference on Solid-State Circuits (A-SSCC). In 2015, he was Chair of the Technical Committee on Circuits and Systems (CAS) of the IEICE. He is a senior member of IEEE.

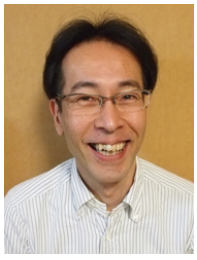

Takeshi Yoshida received the B.E., M.E., and D.E. degrees in electronics engineering from Hiroshima University, Higashi-Hiroshima, Japan, in 1994, 1996, and 2004, respectively. From 1996 to 2001, he was with the System Electronics Laboratories, Nippon Telegraph and Telephone Corporation, Atsugi, Japan. He is currently an Associate Professor with the Graduate School of Advanced Science and Engineering, Hiroshima University. Dr. Yoshida is a member of IEEE.

Minoru Fujishima received his Ph.D. from the University of Tokyo in 1993, and after working as an assistant and associate professor at the University of Tokyo, he has been a full professor at Hiroshima University since 2009. He was a visiting professor at the Katholieke Universiteit Leuven, Belgium, from 1998 to 2000. He was formerly engaged in research on design and modeling of CMOS and BiCMOS circuits, nonlinear circuits, single-electron circuits, and quantum computing circuits, and is currently interested in research on ultrahigh-speed wireless communications using terahertz. He served as a distinguished lecturer of the IEEE Solid State Circuits Society, Chair of the IEEE Japan Council Chapter Operations Committee, and was President of the Electronics Society of the Institute of Electronics, Information and Communication Engineers. He is a senior member of the IEEE, and a member of the Japan Society of Applied Physics.